THE ASTROPHYSICAL JOURNAL, 377:519–525, 1991 August 20

THE DENSE MOLECULAR ENVELOPE AROUND THE COMPACT H II REGION G5.89−0.39 (W28 A2)

YOLANDA GÓMEZ,[1,2] LUIS F. RODRÍGUEZ,[1,2] GUIDO GARAY,[3] AND JAMES M. MORAN[2]

Received 1990 October 9; accepted 1991 February 26

ABSTRACT

We present VLA observations of ammonia in the $(J, K) = (2, 2)$ and (3, 3) inversion transitions toward the compact H II region G5.89−0.39. These observations reveal the presence of a massive ($\sim 30\ M_\odot$) and hot (~ 90 K) molecular envelope that is clumpy and probably undergoing expansion. We also detect overheated or inverted (3, 3) ammonia emission in front of the H II region. The radio continuum map shows bipolar protuberances, suggesting that the ionized gas is flowing out through openings in the molecular envelope.

Subject headings: interstellar: molecules — nebulae: H II regions — radio sources: lines — stars: formation

1. INTRODUCTION

Some observational characteristics, such as the presence of H_2O and OH maser emission and large far-infrared luminosities, are shared by both very young and very evolved stars. These similarities may be due to the fact that in both the early and late stages of stellar evolution, stars are surrounded by massive envelopes of dust and gas. Hence the reliable classification of some objects as either young or evolved stars is sometimes difficult. Examples of sources with ambiguous classification include VY CMa (Lada & Reid 1978), Orion IRc2 (Snyder et al. 1978), G70.7+1.2 (de Muizon et al. 1988), IRAS 17516−2525 (van der Veen et al. 1990), and G5.89−0.39 (Zijlstra & Pottasch 1988).

The source G5.89−0.39 (also known as W28 A2) has been studied in detail at radio and infrared wavelengths. It exhibits OH maser emission in the 1612, 1665, and 1667 MHz transitions (Zijlstra et al. 1990) and H_2O maser emission in the 22,235 MHz transition (e.g., Genzel & Downes 1977; Caswell et al. 1983). In the radio continuum, G5.89−0.39 has a bright, compact ($\theta_s \simeq 5''$), shell-like morphology (Wood & Churchwell 1989; Zijlstra et al. 1990), with an extremely large emission measure, EM $\simeq 5 \times 10^8$ pc cm^{-6} (see below). Analysis of H I absorption indicates that G5.89−0.39 has a distance of between 3 and 7 kpc (Zijlstra et al. 1990) and probably lies in the well-known molecular ring at a distance of about 4 kpc. In this paper we adopt 4 kpc as the distance to G5.89−0.39. At this distance the angular size of the continuum source corresponds to a linear diameter of about 0.1 pc. The emission measure and size give an average electron density of $n_e \sim 7 \times 10^4$ cm^{-3} and an ionized hydrogen mass of $M_{\rm H\,II} \sim 1\ M_\odot$. Observations of the H76α recombination line at 14.7 GHz made with the VLA show a broad, asymmetric feature (Wood & Churchwell 1989). Moreover, observations with higher angular resolution of the same line reveal a velocity gradient across the nebula (Zijlstra et al. 1990). Observations of CO and CS by Harvey & Forveille (1988) show that the radio continuum source is at the center of a compact, dense, and energetic bipolar outflow. The *IRAS* fluxes of G5.89−0.39 (~200, 2200, 13,000, and 27,000 Jy at 12, 25, 60, and 100 μm, respectively) are among the largest in the *IRAS Point Source Catalog* (1985). Based on a distance of 4 kpc, G5.89−0.39 has a luminosity in the 1–1300 μm band of $7 \times 10^5\ L_\odot$ (Chini, Krügel, & Wargau 1987), corresponding to an O5 ZAMS star (Thompson 1984).

There has been doubt as to whether G5.89−0.39 is an H II region or a proto–planetary nebula (Zijlstra & Pottasch 1988). However, the determination of its distance by Zijlstra et al. (1990) and the estimate of its luminosity strongly suggest that it is a compact H II region. In this paper we present observations of excited ammonia, in the $(J, K) = (2, 2)$ and (3, 3) inversion transitions, that reveal the presence of a dense molecular envelope surrounding G5.89−0.39 and provide additional evidence in support of the H II region interpretation.

2. OBSERVATIONS

2.1. *Spectral Observations*

As part of a survey of ultracompact H II regions, we made observations at the Haystack Observatory[4] of the (1, 1) and (3, 3) inversion transition lines of ammonia at 23.69 and 23.87 GHz on 1988 July 4 and February 19, respectively. At these frequencies the half-power beam width was 1.′4, and the aperture efficiency at an elevation of 45° was 0.28. We used a 512 channel digital autocorrelator with a total bandwidth of 16.67 MHz, giving a velocity resolution (unity weighting) of 0.49 km s^{-1}. The observations were made in the total power mode, and the spectra were corrected for atmospheric attenuation and elevation-dependent gain variations. The parameters of the ammonia lines are given in Table 1.

Assuming an LTE ortho-para ratio for the NH_3 molecule and optically thin line emission, we can derive a rotational temperature from the (3, 3) and (1, 1) transitions from the equation (Ho & Townes 1983)

$$T_{\rm ROT}(33\text{–}11) = 101.2\left\{\ln\left[12.5\,\frac{T_A(1,\,1;\,m)}{T_A(3,\,3;\,m)}\right]\right\}^{-1}\ \text{K}\,, \qquad (1)$$

where $T_A(J, K; m)$ represents the corrected antenna temperature of the main group of hyperfine components of the (J, K) transition. From the values of T_A given in Table 1, we

[1] Postal address: Instituto de Astronomía, UNAM, Apdo. Postal 70-264, México City 04510, D.F., México.

[2] Harvard-Smithsonian Center for Astrophysics, 60 Garden Street, Cambridge, MA 02138.

[3] Departamento de Astronomía, Universidad de Chile, Casilla 36-D, Santiago, Chile.

[4] Radio Astronomy at the Haystack Observatory of the Northeast Radio Observatory Corporation is supported by a grant from the National Science Foundation.

TABLE 1

PARAMETERS OF AMMONIA LINES TOWARD G5.89−0.39[a]

Transition	T_A (K)	v_{LSR} (km s^{-1})	Δv (km s^{-1})
NH_3 (1, 1).....	0.51 ± 0.05	9.6 ± 0.2	3.2 ± 0.4
NH_3 (3, 3).....	0.21 ± 0.02	10.1 ± 0.1	3.6 ± 0.3

[a] Single-dish observations made at Haystack Observatory. Coordinates were $\alpha(1950) = 17^h57^m26^s.8$; $\delta(1950) = -24°03'57''$.

find $T_{ROT}(33\text{–}11) \simeq 30$ K, in good agreement with the value of $T_{ROT}(22\text{–}11) \simeq 29$ K derived by Churchwell, Walmsley, & Cesaroni (1990).

2.2. *VLA Observations*

To study the angular distribution of the ammonia emission associated with G5.89−0.39, we made observations of the (2, 2) and (3, 3) ammonia transitions with the VLA of the NRAO[5] during 1988 September 19 and 21. The VLA was in the D-array configuration, and we observed in the spectral line mode with 63 channels of 195.3 kHz (2.5 km s^{-1}) spacing and a total bandwidth of 12.5 MHz. A continuum channel contained the central 75% of the total band. The absolute amplitude calibrator was 3C 286, the phase calibrator was 1730−130, and the bandpass calibrators were 3C 273 and 1730−130. The data were calibrated by applying the complex gain solution from the observations of 3C 286, and the bandpass response was normalized using the observations of 3C 273 and 1730−130. The solution obtained from a self-calibration analysis (Schwab 1980) of the data in the continuum channel was applied to the line channels. The (2, 2) observations (23.72 GHz) were made during poor weather conditions and were noisier by a factor of 2 than the (3, 3) observations (23.87 GHz). The rms noise level in the map of a single spectral line channel made with natural weighting was 15 mJy per beam solid angle for the (3, 3) observations. However, we note that comparison of continuum maps made from both data bases indicates a reliable absolute and relative flux calibration for both sets of data. Since the (3, 3) line observations had better quality, we base most of our discussion on them.

In Figure 1 we show a self-calibrated, cleaned map made with natural weighting from the continuum channel of the (3, 3) data. The ammonia emission is negligible ($\leq$20 mJy beam^{-1}) compared to the continuum emission in this map. The map shows a bright, unresolved core that corresponds to the shell-like structure mapped with higher angular resolution by Wood & Churchwell (1989) and Zijlstra et al. (1990). In addition, the map exhibits protuberances to the northwest and southeast that are also present in the 21 cm, low-angular resolution map ($\sim$18″) of Zijlstra et al. (1990). The total continuum flux densities of the region shown in Figure 1, measured from the bands of the (3, 3) and (2, 2) data, respectively, were 15 ± 1 Jy and 13 ± 1 Jy, suggesting that there may be an error of $\sim$15% in the relative calibration.

Line maps were made from the individual channel maps by subtracting a continuum map made from the average of the off-line channel maps. We made two sets of line maps for each inversion transition. One set was based on the naturally weighted (u, v) data with no taper, which resulted in synthesized beams of 5″.5 × 3″.3 and 6″.5 × 3″.8 for the (2, 2) and (3, 3) observations, respectively. The other set was based on uniformly weighted (u, v) data with a Gaussian taper of 25 kλ, which resulted in synthesized beams of 6″.5 × 5″.2 and 5″.6 × 3″.8 for the (2, 2) and (3, 3) observations, respectively. All spectra were Hanning smoothed to a velocity resolution of 4.9 km s^{-1}. In Figures 2 and 3 we show the individual line maps of the (2, 2) and (3, 3) transitions, made with natural weighting. In these panels we also show a continuum map made with natural weighting from the continuum channel of the (3, 3) data. The maps with more negative velocity are near the edge of our bandpass and have larger noise than the others. We did not detect significant emission at the velocities expected for the inner satellite transition on the low-frequency side of the main transition (the inner satellite on the high-frequency side of the main transition was outside our bandpass). The 3 σ upper limits of 45 mJy beam^{-1} and 90 mJy beam^{-1}, for the (3, 3) and (2, 2) inner satellite emission, respectively, can be used to estimate upper limits on the opacity of $\tau(3, 3; m) < 5$ and $\tau(2, 2; m) < 8$.

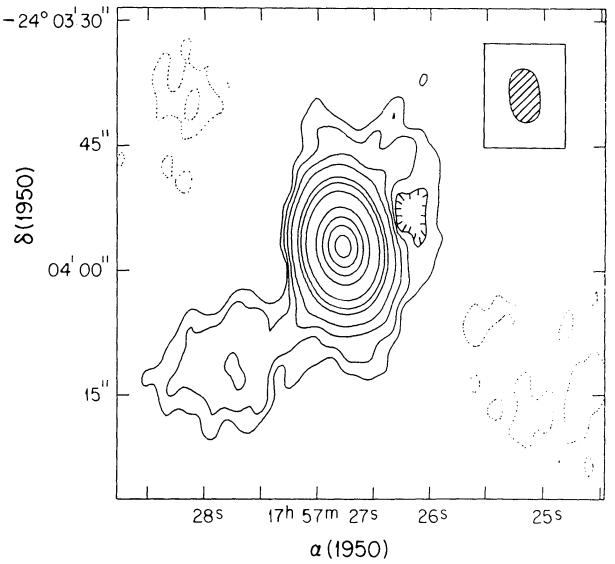

FIG. 1.—Self-calibrated 1.3 cm continuum map of G5.89−0.39 made with the VLA (D-configuration). Beam size is 6″.5 × 3″.8 (*beam in upper right*). Contour levels are −0.003, −0.002, 0.002, 0.003, 0.005, 0.01, 0.03, 0.05, 0.1, 0.3, 0.5, 0.7, and 0.9 of the peak flux of 10.0 Jy beam^{-1}.

3. RESULTS AND DISCUSSION

3.1. *Continuum Measurements*

In Figure 4 we show the continuum spectrum of G5.89−0.39 synthesized from the measurements of Zijlstra et al. (1990), Wood & Churchwell (1989), Handa et al. (1987), Chini et al. (1987), and this paper. From our measurements, we have adopted a flux density of 14 ± 1 Jy at 1.3 cm wavelength. The data were fitted to a homogeneous model of free-free emission. The data point of Chini et al. (1987) at 1.3 mm was not included in the analysis because it may contain a significant contribution from dust emission. Our analysis gives a free-free opacity of 0.21 ± 0.03 at the ammonia frequency of 23.9 GHz, and assuming an electron temperature of 10^4 K, we calculate an average emission measure of (5.0 ± 0.6) × 10^8 cm^{-6} pc. The ionizing flux required is $\sim 2 \times 10^{49}$ s^{-1}, which can be supplied

[5] The National Radio Astronomy Observatory is operated by Associated Universities Inc., under cooperative agreement with the National Science Foundation.

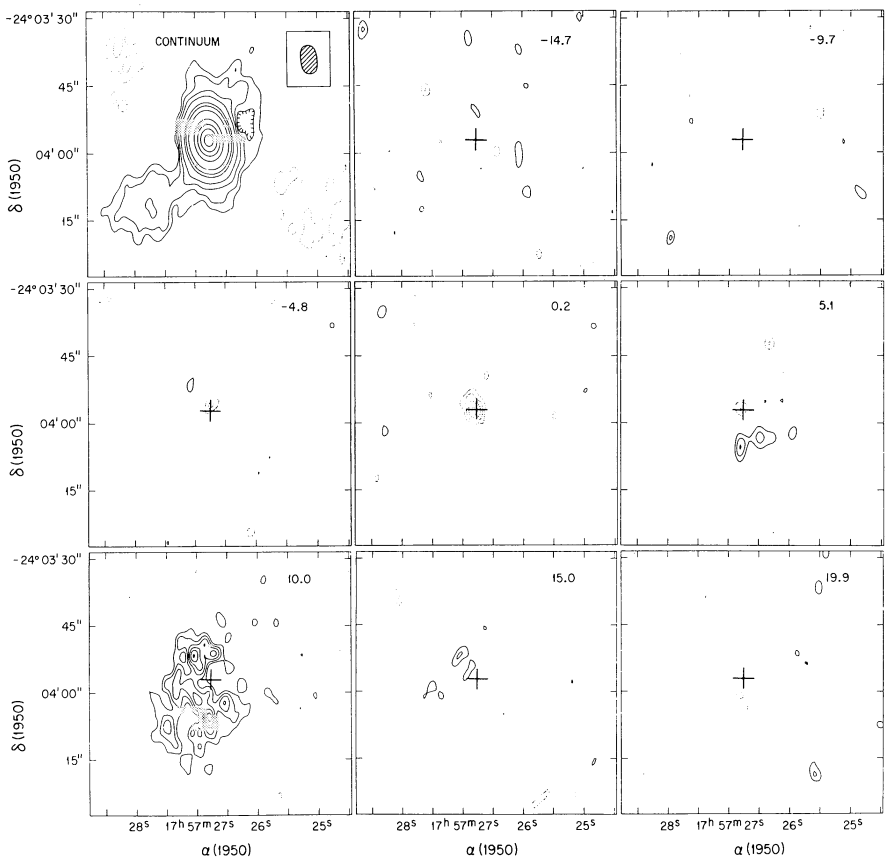

FIG. 2.—Continuum map at 23.87 GHz (*top left corner*) and channel maps of the (2, 2) line of ammonia made with natural weighting. LSR velocity is shown in the right top corner of each line map. Cross indicates the position and size of the compact H II region (5″) taken from Zijlstra et al. (1990). Contour levels for the continuum map are given in Fig. 1. Contour levels for the line maps are −10, −9, −8, −7, −6, −5, −4, −3, 3, 4, 5, 6, 7, 9, and 10 times 30 mJy beam^{-1}.

by an O6 ZAMS star (Thompson 1984). The derived electron density depends on details of the source geometry. The density is about 7×10^4 cm^{-3} for uniform spherical geometry and higher for shell geometry. The protuberances observed to the northwest and southeast in the continuum map shown in Figure 1 probably represent ionized gas that is flowing out through regions where the shell (see map in Zijlstra et al. 1990) is broken. This continuum morphology, a shell-like core with bipolar lobes, is similar to that found in NGC 6334(A) (Rodríguez, Cantó, & Moran 1989). There is also a similarity between G5.89−0.39 and NGC 6334(A) in the kinematics of the ionized gas; both sources have a velocity gradient in the core with magnitude of ~ 10 km s^{-1} and direction perpendicular to the axis of the bipolar structure (Zijlstra et al. 1990; Rodríguez et al.1988).

3.2. *Line Measurements*

The ammonia (2, 2) and (3, 3) line maps made with natural weighting (Figs. 2 and 3) reveal the presence of a remarkable molecular structure surrounding the ionized core. This envelope is particularly evident in the 10.3 km s^{-1} line map of the (3, 3) transition (bottom left corner of Fig. 3), where there is detectable emission over a region with diameter of $\sim 30''$ (~ 0.6 pc). Assuming that a molecular hydrogen density of at least $\sim 10^4$ cm^{-3} is required to excite the (3, 3) ammonia emission, we estimate the mass of this molecular envelope to be ≥ 50 $M_\odot$. However, if there is considerable clumpiness, the mass could be lower. Figure 5 shows the line profiles of the (3, 3) transition over a $24'' \times 24''$ region, based on the line maps made with 25 kλ taper and uniform weighting.

We believe that there are at least two distinct velocity components in the ammonia emission from G5.89−0.39. The first component, which has an average $v_{\rm LSR}$ of 11 ± 0.3 km s^{-1}, engulfs the H II region and is stronger to the southeast. We assume that this component is in LTE, and we estimate its temperature and mass. The second component has $v_{\rm LSR} \simeq 0$ km s^{-1} and appears projected against the H II region. We show that this component is probably out of LTE, and we will discuss its properties separately.

3.2.1. *Gas at* $v_{\rm LSR} \simeq 11$ km s^{-1}

Assuming an LTE ortho-para ratio for the NH_3 molecule and optically thin emission, we can estimate an average rotational temperature from the ratio of the (3, 3) and (2, 2) lines:

$$T_{\rm ROT}(33\text{–}22) = 59.6\left\{\ln\left[3.56\,\frac{S_L(2,\,2;\,m)\,\Delta v(2,\,2;\,m)}{S_L(3,\,3;\,m)\,\Delta v(3,\,3;\,m)}\right]\right\}^{-1} \text{K}\,, \quad (2)$$

where $S_L(J, K; m)$ is the flux density. A fit of a Gaussian profile to the spectrum obtained by integration of the data shown in Figure 5 gives $S_L = 2.3 \pm 0.2$ Jy, $\Delta v = 8.0 \pm 0.8$ km s^{-1}, and $v_{\rm LSR} = 11.4 \pm 0.3$ km s^{-1} for the (3, 3) transition and $S_L = 2.2 \pm 0.3$ Jy, $\Delta v = 4.3 \pm 0.6$ km s^{-1}, and $v_{\rm LSR} = 10.8 \pm 0.3$ km s^{-1}

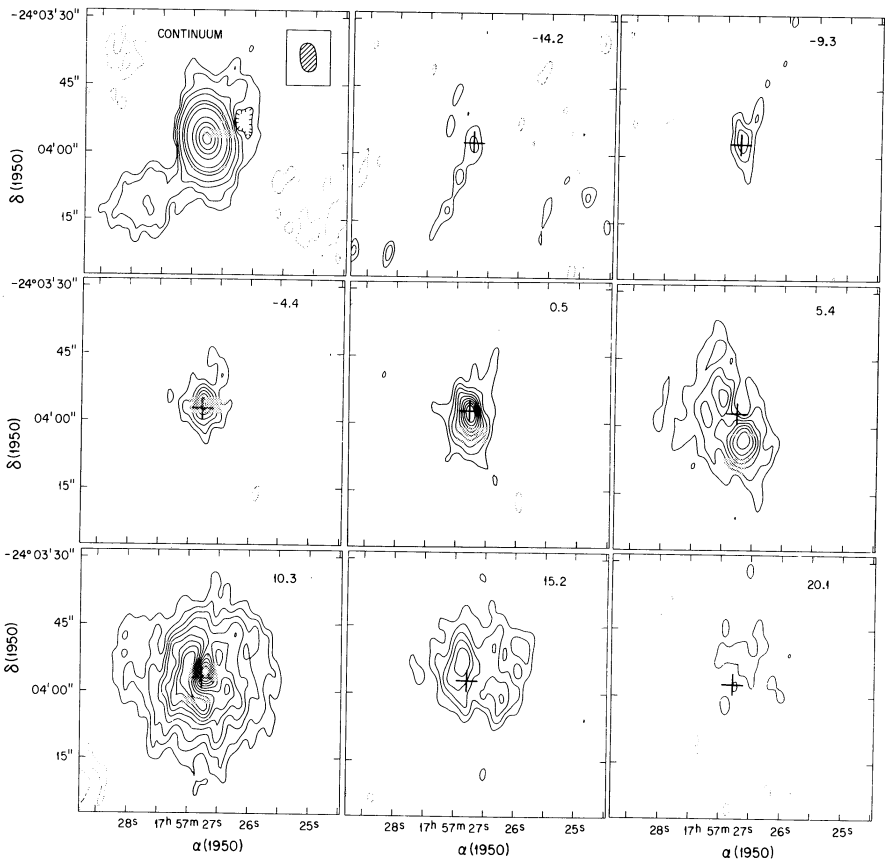

FIG. 3.—Same as Fig. 2, but for the (3, 3) line of ammonia. Contour levels for the line maps are −10, −9, −8, −7, −6, −5, −4, −3, −2, 2, 3, 4, 5, 6, 7, 8, 9, and 10 times 30 mJy beam^{-1}.

for the (2, 2) transition. We note that the spectral width of the (3, 3) emission is significantly broader than that of the (2, 2) emission, suggesting that the (3, 3) emission preferentially samples gas exhibiting larger motions. The rotational temperature derived using the parameters given above is $T_{\rm ROT}(33\text{–}22) \simeq 94 \pm 34$ K, which should be taken as a representative value. We emphasize that this value for the rotational temperature is uncertain because the different widths observed in the (3, 3) and (2, 2) transitions imply that they are not sampling the same gas and because we have observations of only two transitions and our data are thus sensitive to gas with a relatively narrow temperature range. In particular, observations of more highly excited ammonia transitions may reveal the presence of hotter gas.

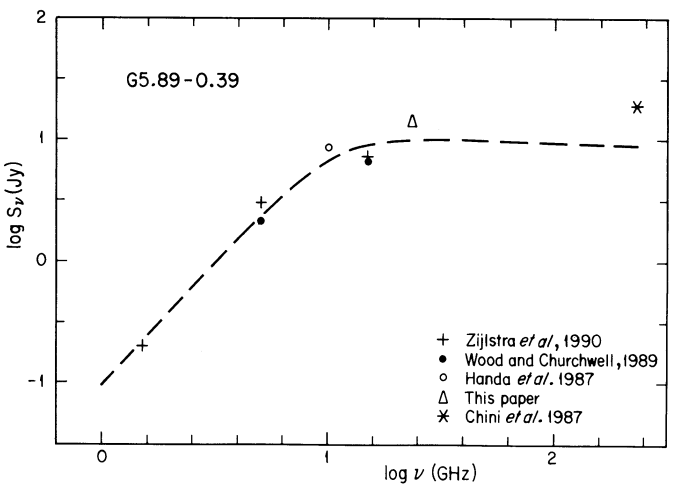

FIG. 4.—Radio continuum flux density vs. frequency for G5.89−0.39. Data were fitted to a model of a plane-parallel free-free emission source. The data point of Chini et al. (1987) was not included in the fit since it may include a significant contribution from dust emission.

We also fitted the (3, 3) spectra obtained by integrating the line flux densities per beam over the three regions labeled "A," "B," and "C" in Figure 5 to Gaussian profiles. The parameters of these fits are given in Table 2. The brightness temperature (col. [5]) is derived from S_L multiplying by 6.3×10^{-2}. The opacity τ of the (3, 3) main line is estimated using the relation $T_L^b = (T_{\rm ex} - T_{\rm bg})(1 - e^{-\tau})$, where $T_{\rm ex}$ is the excitation temperature and $T_{\rm bg}$ is the background temperature. Adopting $T_{\rm bg} = 2.7$ K, $T_{\rm ex} = T_{\rm ROT} \simeq 94$ K, we obtain the opacities given in column [6] of Table 2.

The total column density of NH_3 can be obtained from the optical depth $\tau(J, K)$, and the rotational temperature, assuming an LTE population for all ammonia levels, using the expression

$$N(\mathrm{NH_3}) = \frac{1.65 \times 10^{14} J(J+1)}{\nu g_K K^2 (2J+1)} \Delta v \tau(J, K) Q T_{\rm ex} \exp\left[\frac{E(J, K)}{k T_{\rm ROT}}\right], \quad (3)$$

where ν is the transition frequency in GHz, g_K is the statistical weight ($g_K = 2$ for the ortho states), $E(J, K)$ is the rotational

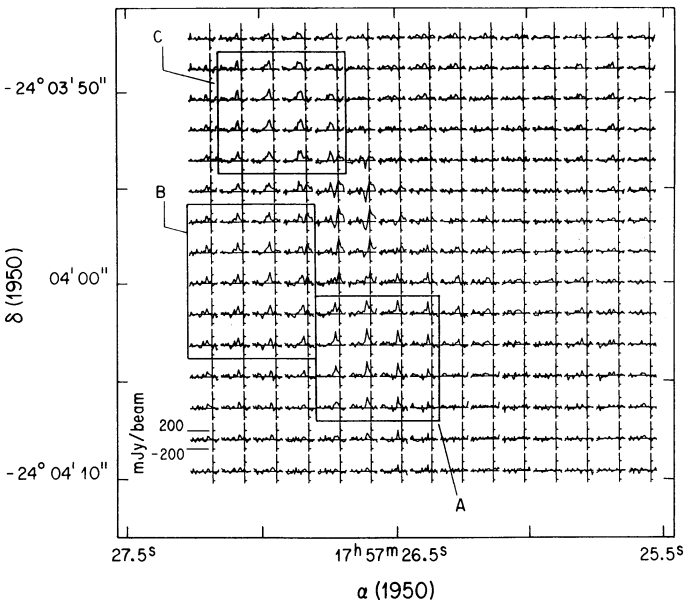

FIG. 5.—Beam-averaged spectral profiles of the (3, 3) line of ammonia made with uniform weighting. Pixel size is 1".6; velocity scale increases from −10.5 to 45.9 km s^{-1}, right to left. Boxes indicate the regions where we averaged the data and fitted Gaussian line profiles.

energy of the (J, K) level above the ground state, Δv is the line width in km s^{-1}, Q is the partition function, and k is Boltzmann's constant. Assuming LTE and for $T_{\rm ROT} \gg 20$ K, we can use the partition function given by (e.g., Genzel et al. 1982)

$$Q = 115\left(\frac{T_{\rm ROT}}{200K}\right)^{3/2} . \quad (4)$$

The total ammonia column densities obtained from equation (3) using $\tau(3, 3) = 1.12\tau(3, 3; m)$ and $T_{\rm ex} = T_{\rm ROT} = 94$ K are given in column [7] of Table 2.

To determine the hydrogen molecular column density, we need to know the ratio $[NH_3]/[H_2]$. This ratio has been estimated to be in the range from 10^{-7} for small and dark clouds (Ungerechts, Walmsley, & Winnewisser 1980) to 10^{-5} in the dense nucleus of the Orion molecular cloud (Genzel et al. 1982). We adopt an average ratio of 10^{-6}. If we also assume that the characteristic length of the regions is equal to the projected size of the overall region, we obtain the molecular hydrogen densities given in Table 2, which are of order 10^4 cm^{-3}. The masses derived for each of the regions are of order of a few solar masses, and the total mass of the whole region is $\sim 30\ M_\odot$. Note that if we had chosen a molecular ratio of 10^{-5}, typical of dense clouds, the mass estimate would drop to $3\ M_\odot$.

The LSR line center velocities of the emission from regions A, B, and C (see Table 2) are noticeably different, which could be due to a gradient of ~ 10 km s^{-1} pc^{-1}. We consider whether or not the envelope is in virial equilibrium. The virial mass for a spherical cloud with a constant density, based on the gravitational and kinetic energy terms, is given by (Mihalas & Routly 1968)

$$\left(\frac{M_{\rm vir}}{M_\odot}\right) = 210\left(\frac{\Delta v}{\rm km\ s^{-1}}\right)^2\left(\frac{R}{\rm pc}\right), \quad (5)$$

where R is the cloud radius and Δv is the FWHM line width. In the 11 km s^{-1} cloud, $R \sim 0.2$ pc and $\Delta v \sim 8$ km s^{-1}, so the mass required for virial equilibrium is $\sim 3 \times 10^3\ M_\odot$. This value exceeds the value of the total mass of the region, which we estimate as follows. The ionized gas mass is $M_{\rm H\,II} \simeq 1\ M_\odot$, while the molecular mass is $M_{\rm H_2} \simeq 30\ M_\odot$. We know that there is at least one O-type star ionizing the region, which we take to be an O5 ZAMS star with a mass of $\sim 30\ M_\odot$ (Mezger, Smith, & Churchwell 1974). The total mass of 61 $M_\odot$ is much smaller than the mass required to bind the motions, which suggests that the molecular cloud is expanding and possibly rotating. On the other hand, if we assume that the total observed luminosity of $\sim 7 \times 10^5\ L_\odot$ is produced by a stellar cluster that follows the IMF of Miller & Scalo (1979) with a minimum mass of 0.6 $M_\odot$, then the cluster mass would be $\sim 2000\ M_\odot$, with ~ 1500 members. However, such a large stellar density (4.5×10^4 star pc^{-3}) is unlikely to occur in the small volume of ~ 0.03 pc^{-3} considered here. For example, in the extreme case of the core of the Orion cluster (Herbig & Terndrup 1986), the stellar density is ~ 20 times smaller. Hence, the molecular gas is likely to be in expansion. Additional evidence favoring expansion comes from Harvey & Forveille (1988), who found a powerful bipolar outflow in the region. Using observations of ^{12}CO and ^{13}CO, they derive a mass of 70 $M_\odot$ for the high-velocity molecular gas. Blueshifted velocities are found to the northwest and redshifted velocities to the southeast. This orientation is similar to the orientation of the protuberances in the continuum map (Fig. 1). The flow traced by the CO and the ionized gas appears to be an extension of the OH bipolar outflow detected at the transitions 1612, 1665, and 1667 MHz by Zijlstra et al. (1990). It should be noted, however, that the presence of outflow does not exclude the possibility of simultaneous accretion. Indeed, several of the scenarios for outflow derive their energy at the expense of accretion (Shu, Adams, & Lizano 1987). Finally, support for the expansion motions of the molecular gas comes from the

TABLE 2

PARAMETERS OF THE (3, 3) EMISSION

	OBSERVED			DERIVED				
REGION (1)	S_L (mJy) (2)	$v_{\rm LSR}$ (km s^{-1}) (3)	Δv (km s^{-1}) (4)	$\langle T_L^b \rangle$ (K) (5)	$\tau(m)$ (6)	$N(NH_3)$ (10^{16} cm^{-2}) (7)	$n(H_2)$ (10^4 cm^{-3}) (8)	$M(H_2)$ ($M_\odot$) (9)
A	400 ± 40	8.8 ± 0.2	4.4 ± 0.5	25 ± 3	0.32	1.2	3.1	3
B	340 ± 50	11.5 ± 0.4	4.5 ± 0.8	17 ± 3	0.21	0.8	1.8	2
C	250 ± 30	12.3 ± 0.5	9.8 ± 1.2	16 ± 2	0.19	1.6	4.2	4
Whole	2300 ± 200	11.4 ± 0.3	8.0 ± 0.8	11 ± 1	0.13	0.9	0.6	30

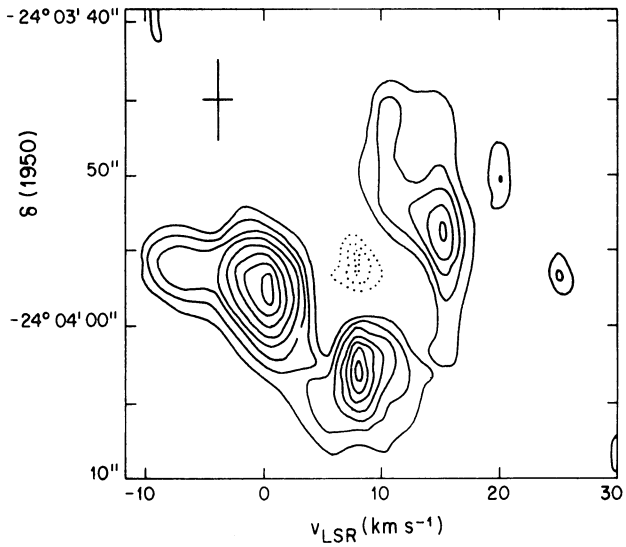

FIG. 6.—Velocity-position map of the NH_3 (3, 3) line, along a north-south direction at $\alpha = 17^h57^m26^s.8$. Contour levels are −8, −7, −6, −5, −4, −3, −2, 2, 3, 4, 5, 6, 7, 8, 9, and 10 times 35 mJy beam^{-1}. Cross in the left top corner indicates the spatial and velocity resolutions (5″ and 0.24 km s^{-1}).

position versus velocity diagram shown in Figure 6. This figure shows a ringlike pattern centered at ~8 km s^{-1} with emission components at ~0 and 16 km s^{-1}. The feature at ~0 km s^{-1} is discussed in detail in the next section. The absorption feature at the center of the pattern, with $v_{LSR} \simeq 8$ km s^{-1}, could be due to ambient gas in the line of sight to the H II region.

In Figure 7 we show in a gray-scale plot the distribution of the brightness temperature ratio $T_L(3, 3)/T_L(2, 2)$ toward the source. This ratio was obtained from the line maps at 10 km s^{-1} made with natural weighting. We can obtain the rotational temperature under the assumption of LTE and optically thin emission. With these assumptions, the darker gray regions show higher temperatures, and the lighter regions represent lower temperatures. From the superposition of the (3, 3)/(2, 2) line ratio map and the (2, 2) ammonia map, one can see that the hot regions do not coincide with the ammonia condensation peaks. This suggests that the medium is clumpy and that the gas around the ammonia condensations is tenuous and warmer.

3.2.2. *Gas at* $v_{LSR} \simeq 0$ km s^{-1}

There is an interesting component at $v_{LSR} \sim 0$ km s^{-1} (see Figs. 2 and 3) where the (2, 2) line appears in absorption and the (3, 3) line appears in emission (see also Fig. 6). We assume that the same gas is responsible for the (2, 2) absorption and the (3, 3) emission. The component appears projected against the H II region. The brightness temperature T_B at 23.8 GHz of the H II continuum emission averaged over our beam (6″.5 × 3″.8) is $T_B \simeq 900$ K. Since $T_L = (T_{ex} - T_B)(1 - e^{-\tau})$, where T_L is the line temperature and T_{ex} is the excitation temperature, then $T_L(2, 2) < 0$ implies that $T_{ex}(2, 2) < T_B \simeq 900$ K. However, since $T_L(3, 3) > 0$, we must have $T_{ex}(3, 3) > T_B \simeq 900$ K. At this kinetic temperature, the ammonia would be dissociated, so we conclude that the excitation temperature is not, in this case, an indicator of the kinetic temperature in the region. The ammonia is probably anomalously excited with the transition undergoing overheating or inversion. A similar situation, with

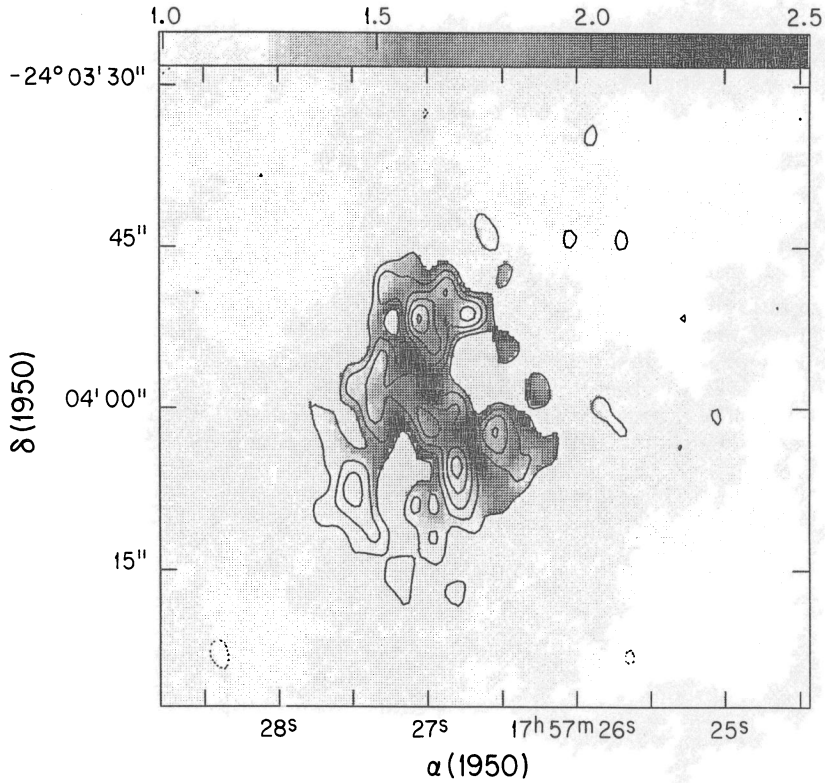

FIG. 7.—Gray-scale plot of the line ratios $T_L(3, 3)/T_L(2, 2)$ superposed on a contour map of the (2, 2) line emission. All data are at $v_{LSR} \simeq 10.0$ km s^{-1}. Gray scale goes from 1.0 to 2.5 (*see top*), and the contours are those given in Fig. 2.

the (2, 2) line in absorption and the (3, 3) line in emission, has been reported in DR 21 (Guilloteau et al. 1983).

Given the apparent anomalous excitation of the ammonia emission, it is unlikely that the ~ 0 km s^{-1} component is a chance coincidence of foreground line-of-sight gas. More probably it is located close to the H II region. Since the emission and absorption are blueshifted by ~ 10 km s^{-1} with respect to the systemic velocity of ~ 10 km s^{-1} and since the gas is in front of the H II region, it is probably part of the outflow.

4. CONCLUSIONS

Using the VLA we observed the compact H II region G5.89−0.39 in the ammonia (2, 2) and (3, 3) inversion transitions. The H II region, with a diameter of 0.1 pc, is embedded in a molecular envelope with a diameter of 0.4 pc. The molecular envelope is hot ($T_K \simeq 90$ K) and massive ($M \simeq 30\ M_\odot$), having a molecular hydrogen density of $\sim 10^4$ cm^{-3}. The molecular gas in the envelope is inhomogeneous and most probably in expansion. The (3, 3) line emission at $v_{\rm LSR} \sim 0$ km s^{-1} exhibits anomalous excitation conditions, suggestive of overheating or inversion. The morphology of the continuum map suggests that the molecular bipolar outflow observed in this source may have a counterpart in the ionized gas.

We thank K. Menten and D. Wood for their helpful comments. Y. G. and L. F. R. acknowledge support from DGAPA-UNAM grant IN010589.

REFERENCES

Caswell, J. L., Batchelor, R. A., Forster, J. R., & Wellington, K. J. 1983, Australian J. Phys., 36, 401
Chini, R., Krügel, E., & Wargau, W. 1987, A&A, 181, 378
Churchwell, E., Walmsley, C. M., & Cesaroni, R. 1990, A&AS, 83, 119
de Muizon, M., Strom, R. G., Oort, M. J. A., Class, J. J., & Braun, R. 1988, A&A, 193, 248
Genzel, R., & Downes, D. 1977, A&AS, 30, 145
Genzel, R., Downes, D., Ho, P. T. P., & Bieging, J. 1982, ApJ, 259, L103
Guilloteau, S., Wilson, T. L., Martin, R. N., Batrla, W., & Pauls, T. A. 1983, A&A, 124, 322
Handa, T., Sofue, Y., Nakai, N., Hirabayashi, H., & Inoue, M. 1987, PASJ, 39, 709
Harvey, P. M., & Forveille, T. 1988, A&A, 107, L19
Herbig, G. H., & Terndrup, D. M. 1986, ApJ, 307, 609
Ho, P. T. P., & Townes, C. H. 1983, ARA&A, 21, 239
IRAS Point Source Catalog. 1985, Joint IRAS Science Working Group (Washington: GPO)
Lada, C. J., & Reid, M. J. 1978, ApJ, 219, 95
Mezger, P. G., Smith, L. F., & Churchwell, E. 1974, A&A, 32, 269
Mihalas, D., & Routly, P. M. 1968, Galactic Astronomy (San Francisco: Freeman)
Miller, G. E., & Scalo, J. M. 1979, ApJS, 41, 513
Rodríguez, L. F., Cantó, J., & Moran, J. M. 1989, ApJ, 333, 801
Rodríguez, L. F., Moran, J. M., Cantó, J., & Kahn, F. D. 1988, BAAS, 20, 1031
Schwab, F. 1980, Proc. SPIE, 231, 18
Shu, F. H., Adams, F. C., & Lizano, S. 1987, ARA&A, 25, 23
Snyder, L. E., Dickinson, D. F., Brown, L. W., & Buhl, D. 1978, ApJ, 224, 512
Thompson, R. I. 1984, ApJ, 283, 165
Ungerechts, H., Walmsley, C. M., & Winnewisser, G. 1980, A&A, 88, 259
van der Veen, W. E. C. J., Geballe, T. R., Habing, H. J., & van Langevelde, H. J. 1990, in preparation
Wood, D. O. S., & Churchwell, E. 1989, ApJS, 69, 831
Zijlstra, A. A., & Pottasch, S. R. 1988, A&A, 196, L9
Zijlstra, A. A., Pottasch, S. R., Engels, D., Roelfsema, P., te Lintel Hekkert, P., & Umana, G. 1990, MNRAS, 246, 217